Hydrogen Evolution by Molecular Photocatalysis 46

Shunichi Fukuzumi, Yong-Min Lee, and Wonwoo Nam

Contents

Abstract

This chapter focuses on photocatalytic mechanisms of hydrogen (H_2) evolution to clarify how photons are converted to two electrons that are required for H_2 production from two protons. A two-electron-reduced metal complex is produced via disproportionation of the one-electron-reduced species of a metal complex produced via photoinduced electron transfer, leading to H_2 evolution. A one-photon two-electron process is made possible in photocatalytic H_2 evolution by combination of thermal and photoinduced electron transfer. Photoexcitation of 9-mesityl-10-methylacridinium ion (Acr^+–Mes) with NADH that is a hydride (two-electrons and a proton) donor resulted in the reduction of two equivalents of Acr^+–Mes to produce two equivalents of $Acr^{\bullet}$-Mes that reduce protons to produce H_2 in the presence of an H_2 evolution catalyst. Acr^+-Mes can also be applied to photocatalytic generation of H_2, accompanied by dehydrogenative oxygenation of an alkene and selective C(sp^2)-H amination of arenes. A one-photon two-electron process is also made possible by a bimolecular reaction of the excited state of a metal-hydride complex with the ground state complex to produce H_2.

Keywords

Electron transfer · Hydrogen evolution · Photocatalysis · Reaction mechanism · Metal-hydride complex

46.1 Introduction

Among clean, renewable alternatives to fossil fuels, hydrogen is one of the most attractive candidates for the future sustainable energy system, because hydrogen is produced via water splitting by directly using solar energy or by electrolysis with a solar cell [1–21]. Hydrogen is used to fix carbon dioxide and to furnish fuels, chemicals, and biomass [22–25]. A photovoltaic (PV) electrolysis of water has already achieved an average solar-to-hydrogen (STH) efficiency as high as 30% under continuous operation [26]. In industry, however, only 4% of hydrogen is currently produced by water electrolysis, whereas steam methane reforming and coal gasification make more than 95% of the

S. Fukuzumi (✉)
Department of Chemistry and Nano Science, Ewha Womans University, Seoul, South Korea

Faculty of Science and Engineering, Meijo University, Nagoya, Aichi, Japan
e-mail: fukuzumi@chem.eng.osaka-u.ac.jp

Y.-M. Lee (✉) · W. Nam (✉)
Department of Chemistry and Nano Science, Ewha Womans University, Seoul, South Korea
e-mail: yomlee@ewha.ac.kr; wwnam@ewha.ac.kr

D. W. Bahnemann, A. O. T. Patrocinio (eds.), *Springer Handbook of Inorganic Photochemistry*, Springer Handbooks,
https://doi.org/10.1007/978-3-030-63713-2_46

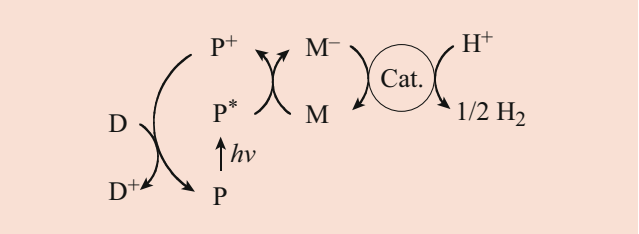

Fig. 46.1 A generalized three component photocatalytic system for hydrogen production where D sacrificial electron donor, P photocatalyst, M electron mediator or relay, and Cat. hydrogen evolving catalyst

whole hydrogen production, because the cost of hydrogen production by electrolysis is still much higher than that produced by fossil fuels [26]. The high cost of hydrogen production by electrolysis results from the use of precious metal such as platinum as the hydrogen evolution catalysts for electrolysis of water [26]. In order to develop more efficient catalysts composed of earth-abundant metals for the hydrogen evolution, it is highly desired to clarify the molecular mechanism of the catalytic hydrogen evolution. In general, the catalytic hydrogen evolution consists of several components as shown in Fig. 46.1, where D = sacrificial electron donor, P = photocatalyst (photosensitizer), M = electron mediator or relay, and Cat. = hydrogen evolving catalyst. Although both photocatalyst and photosensitizer have been used to describe molecules, which participate in light-driven chemical processes without being consumed, the term "photocatalyst" is frequently used to avoid the usage of term "photosensitizer," which is normally used to describe a molecule that participates in energy transfer processes [27–33]. Thus, the term "photocatalyst" instead of "photosensitizer" is used in this chapter. Photocatalysts have been extensively varied ranging from $[Ru^{II}(bpy)_3]^{2+}$ [34–37] to Zn(II) porphyrins [37–39], cyclometalated Ir(III) complexes [40–42], organic dyes [43, 44], Pt(II) terpyridyl complexes [45, 46], Re(I) complexes [47], and Cu(I) complexes [48–51]. Various sacrificial electron donors such as aliphatic and aromatic amines, 1-benzyl-1,4-dihydronicotinamide (BNAH), 1,4-dihydronictinamide adenine dinucleotide (NADH), dimethylphenylbenzimidazoline (BIH), ascorbic acid, oxalate, and thiols have been used for photocatalytic hydrogen evolution [52, 53]. Hydrogen evolving catalysts have also been varied ranging from a colloidal Pt to hydrogenase, hydrogenase model complexes [54–57], iron complexes [58, 59], Ni(II) complexes [60–64], Pt(II) complexes [12, 65, 66], Co(III) complexes [67–70], and Rh(III) complexes [71–74]. This chapter focuses on molecular mechanisms of photocatalytic hydrogen evolution to clarify how photons are converted to two electrons that are required for hydrogen production from two protons.

46.2 Disproportionation Following Photoinduced Electron Transfer

How photoinduced electron transfer of a photocatalyst (a one-electron process) leads to hydrogen evolution (a two-electron process) was clarified for photocatalytic hydrogen evolution with water-soluble transition-metal complexes $[Rh^{III}(Cp^*)(bpy)(H_2O)](SO_4)$ (**1**: $Cp^* = \eta^5$-C_5Me_5, bpy = 2,2′-bipyridine) [75] and $[Ir^{III}(Cp^*)(H_2O)(bpm)Ru^{II}(bpy)_2](SO_4)_2$ (**2**: bpm = 2,2′-bipyrimidine) [76], as proton reduction catalysts, $[Ru^{II}(bpy)_3]^{2+}$ as a photocatalyst and sodium ascorbate (HA^-) as a sacrificial electron donor [77]. Upon photoexcitation of an aqueous solution containing $[Ru^{II}(bpy)_3]^{2+}$, HA^- and $[Rh^{III}(Cp^*)(bpy)]^{2+}$, electron transfer from HA^- to $[Ru^{II}(bpy)_3]^{2+}$ occurred to produce $HA^{\bullet}$ and $[Ru^{I}(bpy)_3]^{+}$, which were detected as transient absorption spectra [77]. The decay of $[Ru^{I}(bpy)_3]^{+}$ (λ_{max} = 510 nm) was accompanied by formation of $[Rh^{II}(Cp^*)(bpy)]^{+}$ (λ_{max} = 750 nm), indicating that electron transfer from $[Ru(bpy)_3]^{+}$ to $[Rh^{III}(Cp^*)(bpy)]^{2+}$ occurred to produce $[Rh^{II}(Cp^*)(bpy)]^{+}$, accompanied by regeneration of $[Ru^{II}(bpy)_3]^{2+}$ (Fig. 46.2a) [77]. The decay of transient absorption spectrum at 510 nm due to $[Ru^{I}(bpy)_3]^{+}$ obeyed pseudo-first-order kinetics, and the pseudo-first-order rate constant increases linearly with concentration of **1**(SO_4) and the rate constant of electron transfer from $[Ru(bpy)_3]^{+}$ to **1**(SO_4) was determined to be $1.3 \times 10^9\ M^{-1}\ s^{-1}$ [77]. In contrast, the decay of $[Rh^{II}(Cp^*)(bpy)]^{+}$ (λ_{max} = 750 nm) obeyed second-order kinetics (Fig. 46.2b), which indicates that disproportionation of $[Rh^{II}(Cp^*)(bpy)]^{+}$ occurred to produce $[Rh^{III}(Cp^*)(bpy)]^{2+}$ and the Rh^{I} complex, $[Rh^{I}(Cp^*)(bpy)]$ [77]. The resulting Rh^{I} complex is immediately protonated at pH 3.6 to produce the Rh(III)-hydride complex, ($[Rh^{III}(Cp^*)(H)(bpy)]^{+}$), which reacts with a proton to generate hydrogen, accompanied by regeneration of $[Rh^{III}(Cp^*)(bpy)]^{2+}$ [77]. Thus, photoinduced electron transfer from HA^- to $[Ru^{II}(bpy)_3]^{2+*}$ (a one-electron process) leads to the two-electron reduction of protons to produce H_2 by disproportionation of the one-electron-reduced species of $[Rh^{III}(Cp^*)(bpy)]^{2+}$ to afford the two-electron-reduced metal complexes ($[Rh^{I}(Cp^*)(bpy)]$), which is protonated to give the metal hydride complex ($[Rh^{III}(Cp^*)(H)(bpy)]^{+}$), as shown in Fig. 46.3 [77]. H_2 is produced by the reaction of $[Rh^{III}(Cp^*)(H)(bpy)]^{+}$ with H^+ to regenerate $[Rh^{III}(Cp^*)(bpy)]^{2+}$ [77]. Such a disproportionation of Rh(II) complexes has been well established for Rh(II) porphyrins to produce Rh(III) and Rh(I) porphyrins [78]. Rh(I) porphyrins react with proton to afford Rh(III)-hydride porphyrins that react further with proton to produce hydrogen and Rh(III) porphyrins [79]. It was also reported that $[Rh^{I}(dmbpy)_2]^{+}$ (dmbpy = 4,4′-dimethyl-2,2′-bipyridine) reacts with protons to form a Rh(III) hydride intermediate that can, in turn, release H_2 [79, 80].

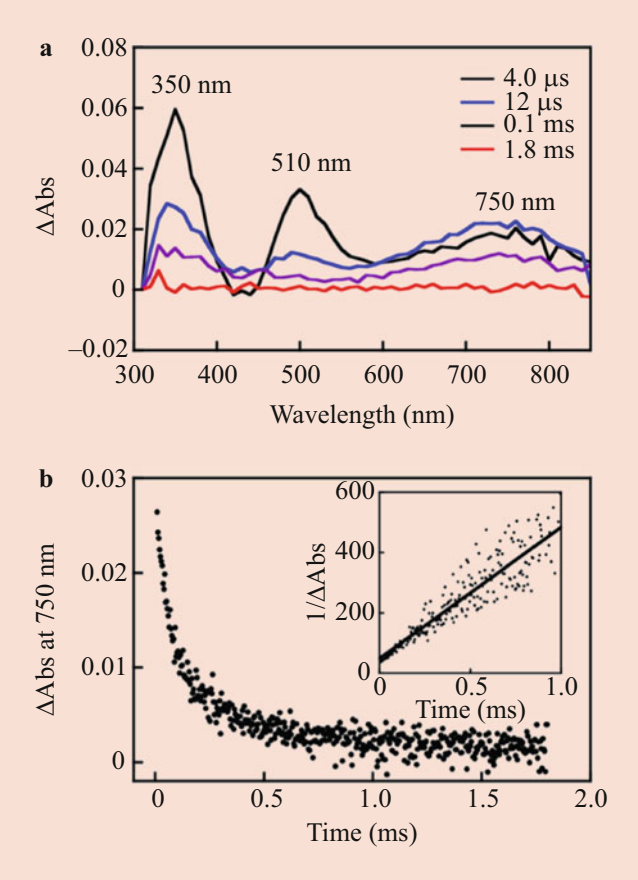

Fig. 46.2 (**a**) Transient absorption spectra of **1** (1.6×10^{-4} M), $[Ru^{II}(bpy)_3]^{2+}$ (8.0×10^{-5} M), H_2A (0.8 M), and NaHA (0.3 M) in deaerated H_2O at pH 3.6 at 298 K after laser excitation at 455 nm. (**b**) Decay time profile of absorbance at 750 nm due to $[Rh^{II}(Cp^*)(bpy)]^+$. Inset shows second-order plot of 1/ΔAbs versus time. (Reprinted with permission from Ref. [77]. Copyright 2011, Wiley-VCH)

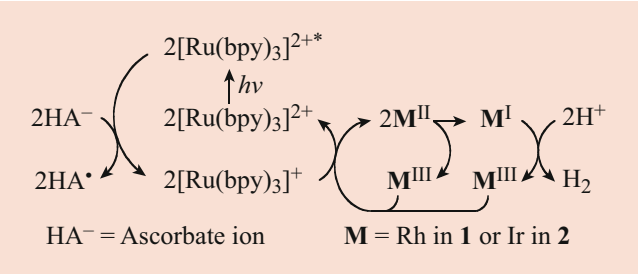

Fig. 46.3 Photocatalytic mechanism for hydrogen evolution form ascorbate (HA^-) with $[Ru^{II}(bpy)_3]^{2+}$ as a photocatalyst and $[Rh^{III}(Cp^*)(bpy)(H_2O)](SO_4)$ (**1**) or $[Ir^{III}(Cp^*)(H_2O)(bpm)Ru^{II}(bpy)_2](SO_4)_2$ (**2**) as a hydrogen evolution catalyst via disproportionation of the one-electron reduced species of **1** or **2**. (Reprinted with permission from Ref. [77]. Copyright 2011, Wiley-VCH)

When $[Ir^{III}(Cp^*)(H_2O)(bpm)Ru^{II}(bpy)_2]^{3+}$ (**2**) was employed as a hydrogen evolution catalyst, photoinduced electron transfer from HA^- to $[Ru^{II}(bpy)_3]^{2+}$ was also followed by electron transfer from $[Ru^{I}(bpy)_3]^+$ to $[Ir^{III}(Cp^*)(H_2O)(bpm)Ru^{II}(bpy)_2]^{3+}$ and disproportionation of $[Ir^{II}(Cp^*)(H_2O)(bpm)Ru^{II}(bpy)_2]^{3+}$ to produce $[Ir^{I}(Cp^*)(H_2O)(bpm)Ru^{II}(bpy)_2]^{2+}$ that reacts with protons to release H_2 [77]. The maximum quantum yield of the photocatalytic hydrogen evolution with **2** (0.015) was obtained at pH 3.6. This is because HA^- acts as an electron donor at pH < 4.0 and the Ir(III)-hydride complex ($[Ir^{III}(Cp^*)(H)(bpm)Ru^{II}(bpy)_2]^{3+}$) is deprotonated at pH >4.0 to produce the low-valent iridium complex $[Ir^{I}(Cp^*)(H_2O)(bpm)Ru^{II}(bpy)_2]^{2+}$, which has no catalytic activity for hydrogen evolution [77].

46.3 Photoinduced Electron Transfer Combined with Thermal Electron Transfer

A one-photon two-electron process was made possible in photocatalytic H_2 evolution with ascorbate (HA^-) and a cobalt(II) chlorin complex ($Co^{II}(Ch)$) via electron transfer from ascorbate to the excited state of $[Ru^{II}(bpy)_3]^{2+}$ followed by electron transfer from $[Ru^{I}(bpy)_3]^+$ to $[Co^{II}(Ch)]$ with proton to give the hydride complex ($Co^{III}(H)(Ch)$), which reacts with proton to produce H_2 as shown in Fig. 46.4. $[Co^{III}(Ch)]^+$ produced by the reaction of ($Co^{III}(H)(Ch)$) with proton was reduced by ascorbate to regenerate $Co^{II}(Ch)$ to complete the catalytic cycle [81]. Thus, once one photon is used to produce $[Co^{I}(Ch)]^-$ from $[Co^{II}(Ch)]$ and another electron is provided by HA^- to regenerate $[Co^{II}(Ch)]$ from $[Co^{III}(Ch)]^+$. Photoexcitation of $[Ru^{II}(bpy)_3]^{2+}$ resulted in electron transfer from AH^- to $[Ru^{II}(bpy)_3]^{2+*}$ to produce $[Ru^{I}(bpy)_3]^+$, followed by electron transfer from $[Ru^{I}(bpy)_3]^+$ to $Co^{II}(Ch)$ to produce $[Co^{I}(Ch)]^-$, which reacts with AH_2 to produce $[Co^{III}(H)(Ch)(AH)]^-$ [81]. The rate constant of electron transfer from $[Ru^{I}(bpy)_3]^+$ to $Co^{II}(Ch)$ was determined to be $2.5 \times 10^9\ M^{-1}\ s^{-1}$. Hydrogen is produced by the reaction of $[Co^{III}(H)(Ch(AH))]^-$ with AH_2 via the Co–H bond heterolysis to produce $[Co^{III}(Ch)(AH)]$, which is reduced by AH^- to regenerate $Co^{II}(Ch)$ [81]. The rate constant of electron transfer from AH^- to $[Co^{III}(Ch)]^+$ that was prepared by the electron-transfer oxidation of $Co^{II}(Ch)$ by $(p\text{-}BrC_6H_4)_3N^{\bullet+}SbCl_6^-$ in H_2O/MeCN was determined to be $1.5 \times 10^3\ M^{-1}\ s^{-1}$. The Co-H bond heterolysis is involved in the rate-determining step, because the kinetic isotope effect ($k_H/k_D = 1.8$) was observed for the photocatalytic hydrogen evolution, when H_2O was replaced by D_2O [81]. Such heterolytic cleavage of the Co-H bond by proton affords H_2 [82].

Virtually the same mechanism as Fig. 46.4 is applied to the photocatalytic H_2 evolution from AH^- with $[Ru^{II}(bpy)_3]^{2+}$ and a water-soluble cobaltous meso-tetrakis (*p*-sulfonylphenyl)porphyrin complex (Co^{II}TPPS) [83]. The best quantum yield of photocatalytic H_2 evolution was

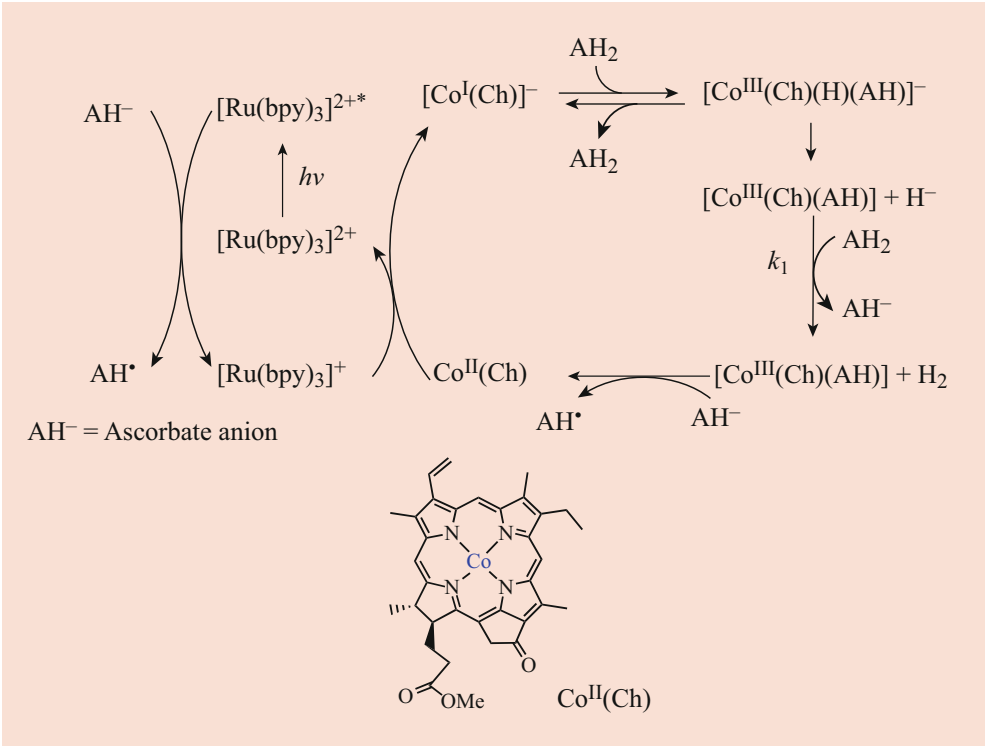

Fig. 46.4 Mechanism of photocatalytic hydrogen evolution from ascorbate (AH^-) and ascorbic acid (AH_2) with $[Ru^{II}(bpy)_3]^{2+}$ and $Co^{II}(Ch)$. (Reprinted with permission from Ref. [81]. Copyright 2015, Royal Society of Chemistry)

obtained as 56% using a cobalt(II) tripodal iminopyridine complex $[Co^{II}(tachpy_3)](ClO_4)_2$ (tachpy$_3$ = *cis*,*cis*-1,3,5-tris (pyridine-2- carboxaldimino)cyclohexane) as a catalyst, a cyclometallated Ir complex as photosensitizer and triethylamine as a sacrificial electron donor in aqueous acetonitrile [84].

46.4 Photoinduced Electron Transfer Followed by Proton and Electron Transfer

A highly efficient photocatalytic hydrogen-evolution system has been constructed using 9-mesityl-10-methylacridinium ion (Acr^+–Mes) [85], poly(N-vinyl-2- pyrrolidone)-protected platinum nanoclusters (Pt-PVP), and NADH (1,4-nicotinamide adenine dinucleotide), used as an organic photoredox catalyst, a hydrogen-evolution catalyst, and an electron donor, respectively [86]. Photoexcitation of Acr^+–Mes results in efficient electron transfer from the Mes moiety to the singlet excited state of the Acr^+ moiety to produce the electron-transfer (ET) state, $Acr^•$–$Mes^{•+}$, which has the strong oxidizing ability of the $Mes^{•+}$ moiety with E_{red} vs. SCE = 2.06 V and the strong reducing ability of the $Acr^•$ moiety with E_{ox} vs. SCE = −0.57 V [87–89]. NADH is oxidized by electron transfer from the $Mes^{•+}$ moiety of $Acr^•$–$Mes^{•+}$ to produce $NADH^{•+}$ and $Acr^•$–Mes as shown in Fig. 46.5, where $NADH^{•+}$ undergoes deprotonation to produce $NAD^•$ that has the strong reducing ability with E_{red} vs. SCE = −1.1 V [90]. The formation of $Acr^•$–Mes is clearly seen as the transient absorption at λ_{max} = 520 nm in Fig. 46.6a, where the increase in bleaching results from a decrease in absorption at 420 nm due to $NAD^•$, accompanied by increase in absorbance at 520 nm due to $Acr^•$–Mes (Fig. 46.6b) [86]. This indicates that electron transfer from $NAD^•$ to Acr^+–Mes occurs to produce NAD^+ and $Acr^•$–Mes. The rate constant of electron transfer from $NAD^•$ to Acr^+–Mes was determined to be 3.7×10^9 M^{-1} s^{-1}, which is close to the diffusion-limited value, as expected from the large driving force (0.53 eV) of electron transfer from $NAD^•$ (E_{ox} = −1.1 V vs. SCE) [90] to the Acr^+ moiety in Acr^+–Mes (E_{red} = −0.57 V vs. SCE) [86]. Thus, one photon used to excite Acr^+–Mes is converted to two electrons that are used to reduce two equivalents of Acr^+–Mes to produce two equivalents of $Acr^•$-Mes (Fig. 46.5) [86]. The quantum yield for the formation of $Acr^•$–Mes was determined to be 0.52 from the absorbance at 520 nm due to the $Acr^•$ moiety [86].

Electron injection from $Acr^•$-Mes produced by the photochemical reduction of Acr^+–Mes to Pt-PVP (PVP = poly (vinylpyrrolidone)) with protons resulted in generation of 0.5 equivalent of hydrogen (Eq. 46.1) as shown in Fig. 46.7 [86]. The hydrogen-evolution rate agrees with the rate of formation of Acr^+–Mes (Fig. 46.8) [91]. This indicates that electron transfer from $Acr^•$–Mes to Pt-PVP is the rate-determining step of the hydrogen-evolution reaction [91].

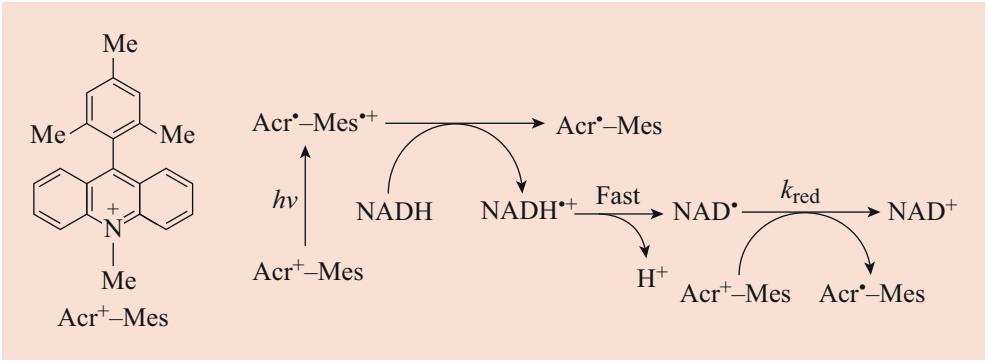

Fig. 46.5 One-photon two-electron processes started from photoinduced electron transfer from the Mes moiety to the singlet excited state of Acr^+-moiety in Acr^+–Mes as an organic photoredox catalyst and NADH as a source of two electrons and protons. (Reprinted with permission from Ref. [86]. Copyright 2007, Royal Society of Chemistry)

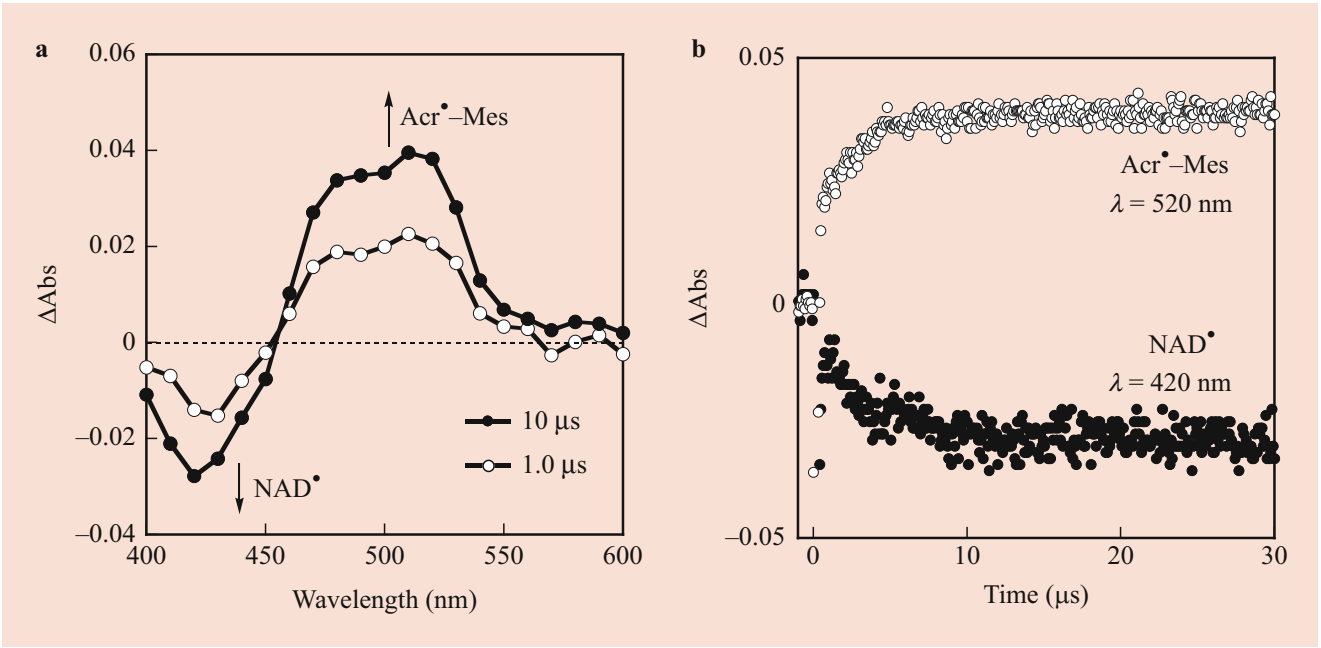

Fig. 46.6 (**a**) Transient absorption spectra of Acr^+–Mes (0.10 mM) and NADH (1.0 mM) in deaerated H_2O and MeCN (v/v 1:1) solution mixture (2.0 cm^3) at 298 K taken at 1.0 μs (○) and 10 μs (●) after nanosecond laser excitation at 430 nm. (**b**) Time profiles of formation of $Acr^•$–Mes at 520 nm and decay of $NAD^•$ at 420 nm. (Reprinted with permission from Ref. [86]. Copyright 2007, Royal Society of Chemistry)

$$2Acr^• - Mes + 2H^+ \xrightarrow[Pt\text{-}PVP]{} 2Acr^+ - Mes + H_2 \qquad (46.1)$$

When a CH_3COOH/CH_3COONa buffer (pH 4.5, 50 mM) in H_2O is replaced by a CH_3COOD/CH_3COONa buffer in D_2O, a substantial inverse kinetic isotope effect (KIE = $k_{et}(H)/k_{et}(D)$ = 0.47) is observed in the rate constant of electron transfer from $Acr^•$–Mes to Pt-PVP (red circles for D^+ and black circles for H^+ in Fig. 46.8b) [91]. Such an inverse kinetic isotope effect results from the higher zero point energy of the Pt–H bond formation than the Pt–D bond formation on Pt-PVP [91]. Because the ET rate increases linearly with increasing $[H^+]$ and $[D^+]$ (Fig. 46.8), ET from $Acr^•$–Mes to PtNPs is coupled with proton transfer (PT) and the proton-coupled electron transfer (PCET) results in formation of a Pt–H bond on the Pt-PVP surface as shown in Fig. 46.9, where H_2 is evolved by reductive elimination from two Pt–H species [91].

Pt nanoparticle catalysts can be replaced by non-Pt metal nanoparticles (MNPs: M = Ru or Ni) for the photocatalytic hydrogen evolution with 2-phenyl-4-(1-naphtyl)-quinolinium ion ($QuPh^+$–NA) as an organic photocatalyst [92] and NADH as a sacrificial electron donor as shown in Fig. 46.10 [93, 94]. Electron transfer from the photogenerated $QuPh^•$–NA to MNPs results in hydrogen evolution even under basic conditions (pH 10) [93, 94]. The catalytic

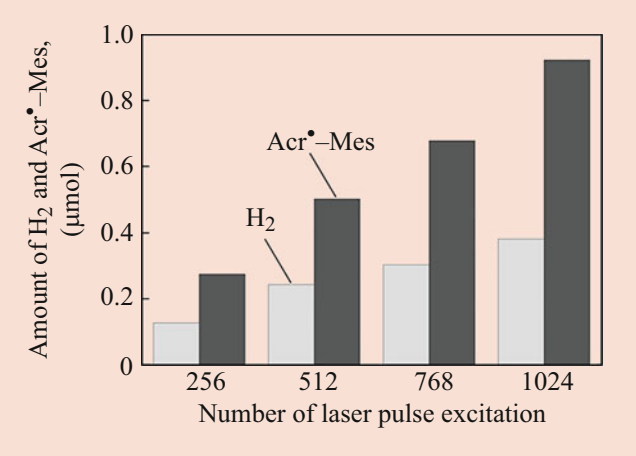

Fig. 46.7 Comparison of the amount of evolved hydrogen and $Acr^{\bullet}$–Mes after laser excitation ($\lambda = 430$ nm) of a deaerated mixed solution (2.0 cm^3) of phthalic acid buffer (pH 4.5; 50 mM) and MeCN [1:1 (v/v)] containing Acr^{+}–Mes (0.10 mM), NADH (2.0 mM) and Pt–PVP (0.10 mg cm^{-3}) at 298 K. (Reprinted with permission from Ref. [86]. Copyright 2007, Royal Society of Chemistry)

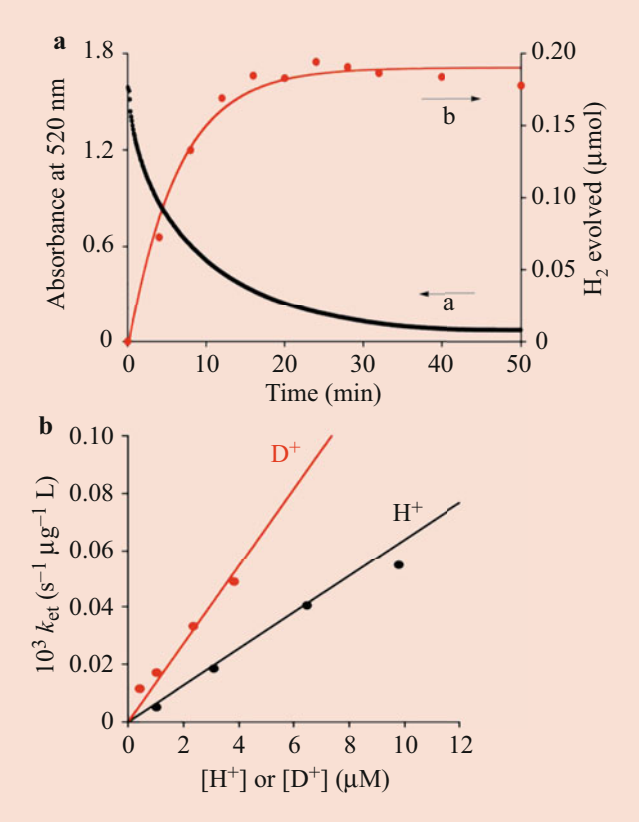

Fig. 46.8 (**a**) Decay time profile (black circles) of absorbance at 520 nm due to $Acr^{\bullet}$–Mes in electron transfer from $Acr^{\bullet}$–Mes to Pt-PVP (0.1 μg) in a (pH 5.0, 50 mM) CH_3COOH/CH_3COONa buffer and MeCN (v/v 1:1) solution mixture. Red circles show time course of hydrogen evolution. (**b**) Dependence of k_{et} on [H^+] (black circles) and [D^+] (red circles) observed in electron transfer from $Acr^{\bullet}$–Mes to Pt-PVP in H_2O/MeCN (v/v 1:1) containing CH_3COOH/CH_3COONa buffer (50 mM) and in D_2O/MeCN (v/v 1:1) containing CH_3COOD/CH_3COONa buffer (50 mM) at 298 K, respectively. (Reprinted with permission from Ref. [91]. Copyright 2010, Wiley-VCH)

activity of RuNPs is as high as that of PtNPs in the photocatalytic hydrogen evolution [93]. The hydrogen evolution rate with the most active Ni nanoparticles (NiNPs; hexagonal close-packed structure, 6.6 nm) examined reached 40% of that with commercially available Pt nanoparticles (2 nm) using the same catalyst weight [94]. In this case as well, a one-photon two-electron process occurs via photoinduced electron transfer from NADH to $QuPh^{\bullet}$–$NA^{\bullet+}$, followed by electron transfer from $NAD^{\bullet}$, which is formed by deprotonation of $NADH^{\bullet+}$, to $QuPh^{+}$–NA to produce two equivalents of $QuPh^{\bullet}$–NA that inject two electrons to MNPs (M = Ru and Ni) with two protons to evolve H_2 (Fig. 46.10) [93, 94]. The rate constants of electron transfer from NADH to $QuPh^{\bullet}$–$NA^{\bullet+}$ and from $NAD^{\bullet}$ to $QuPh^{+}$–NA were determined to be 5.7×10^9 M^{-1} s^{-1} and 2.5×10^9 M^{-1} s^{-1}, respectively. The more negative one-electron reduction potential of the $QuPh^{+}$ moiety in $QuPh^{+}$–NA ($E_{red} = -0.90$ *V* vs. SCE) [92] than that of the Acr^{+} moiety in Acr^{+}–Mes ($E_{red} = -0.57$ V vs. SCE) [86] resulted in efficient H_2 evolution even under basic conditions such as pH 10 [93].

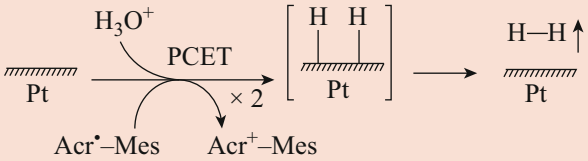

Fig. 46.9 Hydrogen evolution via PCET from $Acr^{\bullet}$–Mes to Pt-PVP. (Reprinted with permission from Ref. [91]. Copyright 2010, Wiley-VCH)

46.5 Photoinduced Electron Transfer Followed by Bond Cleavage

Oxalate is also used as a two-electron donor for photocatalytic H_2 generation with $QuPh^{+}$–NA and Pt-PVP [95]. As the case of oxidation of NADH by $Acr^{\bullet}$–$Mes^{\bullet+}$ (Fig. 46.5), a one photon-two electron process occurs via photoinduced electron transfer from $(COO)_2^{2-}$ to $QuPh^{\bullet}$–$NA^{\bullet+}$ to produce $(COO)_2^{\bullet-}$ and $QuPh^{\bullet}$–NA (Fig. 46.11) [95]. The C–C bond cleavage of $(COO)_2^{\bullet-}$ occurs rapidly to produce CO_2 and $CO_2^{\bullet-}$ that reduced another molecule of $QuPh^{+}$–NA to produce $QuPh^{\bullet}$–NA (Fig. 46.11) [95]. Thus, two equivalents of $QuPh^{\bullet}$–NA obtained by the ET reduction of $QuPh^{+}$–NA with two electrons released from $(COO)_2^{2-}$ (Eq. 46.2) are used to produce H_2 with metal nanoparticles

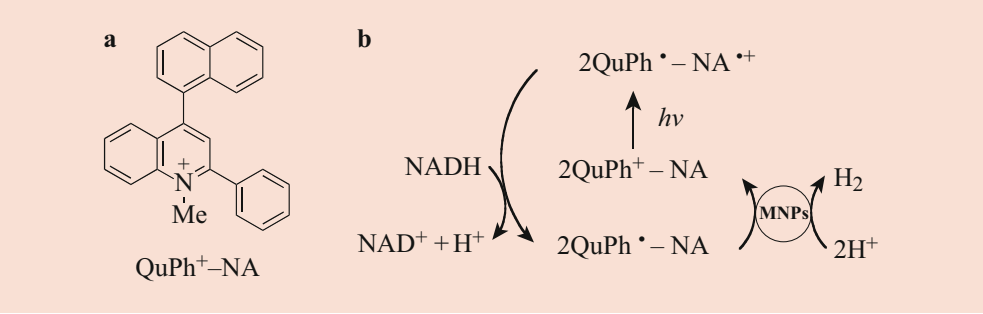

Fig. 46.10 Structure of $QuPh^+$–NA (**a**) and the overall catalytic cycle (**b**) for the photocatalytic hydrogen evolution with NADH and $QuPh^+$–NA and metal nanoparticles (MNPs, M = Ru and Ni). (Reprinted with permission from Ref. [94]. Copyright 2012, Royal Society of Chemistry)

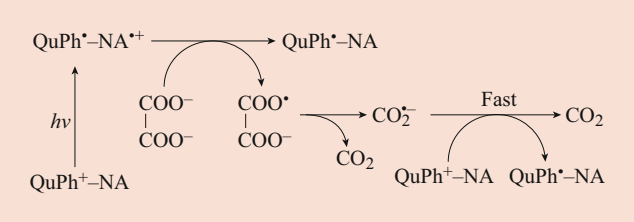

Fig. 46.11 One-photon two-electron processes started from photoinduced electron transfer from the NA moiety to the singlet excited state of $QuPh^+$-moiety in $QuPh^+$–NA as an organic photoredox catalyst and oxalate as a source of two electrons. (Reprinted with permission from Ref. [95]. Copyright 2012, Royal Society of Chemistry)

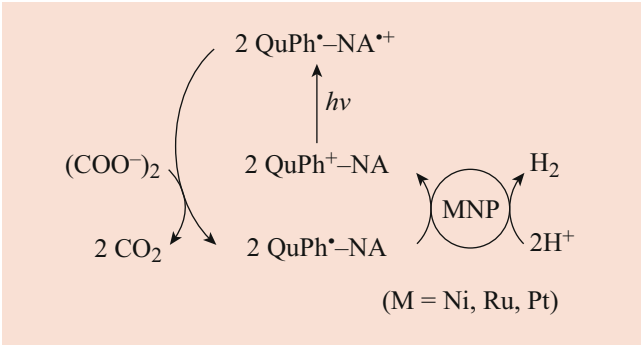

Fig. 46.12 The overall catalytic cycle for the photocatalytic hydrogen evolution with oxalate and $QuPh^+$–NA and metal nanoparticles (MNPs, M = Ru, Ni and Pt). (Reprinted with permission from Ref. [95]. Copyright 2012, Royal Society of Chemistry)

(MNPs) as shown in Fig. 46.12 [95]. The maximum turnover number of H_2 based on $QuPh^+$–NA reached more than 260 [95].

$$(COO)_2^{2-} \rightarrow 2CO_2 + 2e^- \qquad (46.2)$$

A similar one-photon two-electron process occurs for photocatalytic oxidation of water using persulfate ($S_2O_8^{2-}$) as a sacrificial electron acceptor [96]. Electron transfer reduction of $S_2O_8^{2-}$ results in S–S bond cleavage to produce SO_4^{2-} and $SO_4^{\bullet-}$ that act as a much stronger electron acceptor than $S_2O_8^{2-}$, when $S_2O_8^{2-}$ acts as a two-electron oxidant (Eq. 46.3) [96]. Thus, the maximum quantum efficiency for photocatalytic oxidation of water using $S_2O_8^{2-}$ as a sacrificial electron acceptor is 200% via a one photon-two electron process. In fact, incorporation of a small amount of Ca^{2+} ions into a polymeric cobalt cyanide complex to form $Ca_x[Co^{II}(H_2O)_2]_{1.5-x}[Co^{III}(CN)_6]$ resulted in a significant enhancement of activity for photocatalytic water oxidation in a buffer solution (pH 7.0) containing $[Ru^{II}(bpy)_3]^{2+}$ as a photocatalyst and $Na_2S_2O_8$ as an electron acceptor to achieve a quantum efficiency of 200% [97].

$$S_2O_8^{2-} \rightarrow 2SO_4^{2-} - 2e^- \qquad (46.3)$$

46.6 Photoinduced Electron Transfer Followed by Bond Formation

A one photon-two electron process also occurs via photoinduced electron transfer followed by bond formation. For example, photoinduced electron transfer from benzene to the singlet excited state of a photocatalyst (e.g., 3-cyano-1-methylquinolinium ion; $QuCN^+$) occurs to produce benzene radical cation and $QuCN^{\bullet}$, followed by the addition of a nucleophile ($X^- = OH^-$ and NHR^-) to benzene radical cation to give the adduct ($C_6H_6X^{\bullet}$) as shown in Fig. 46.13 [98]. In the presence of $Co^{II}(dmgBF_2)_2$ (dmg = dimethylglyoximate), electron transfer from $C_6H_6X^{\bullet}$ to $Co^{II}(dmgBF_2)_2$ occurs to produce C_6H_5X after deprotonation and $Co^{I}(dmgBF_2)_2$ that reacts with two protons to produce H_2 to generate $[Co^{III}(dmgBF_2)_2]^+$ [98]. Electron transfer from $QuCN^{\bullet}$ to $[Co^{III}(dmgBF_2)_2]^+$ occurs to regenerate $QuCN^+$ and $Co^{II}(dmgBF_2)_2$ to complete the photocatalytic cycle in Fig. 46.13 [98]. Photoinduced electron transfer from benzene to $^1QuCN^{+*}$ is energetically feasible, because the one-electron reduction potential of $^1QuCN^{+*}$ (E_{red} vs. SCE = 2.72 V) [99] is more positive than the one-electron oxidation potential of benzene

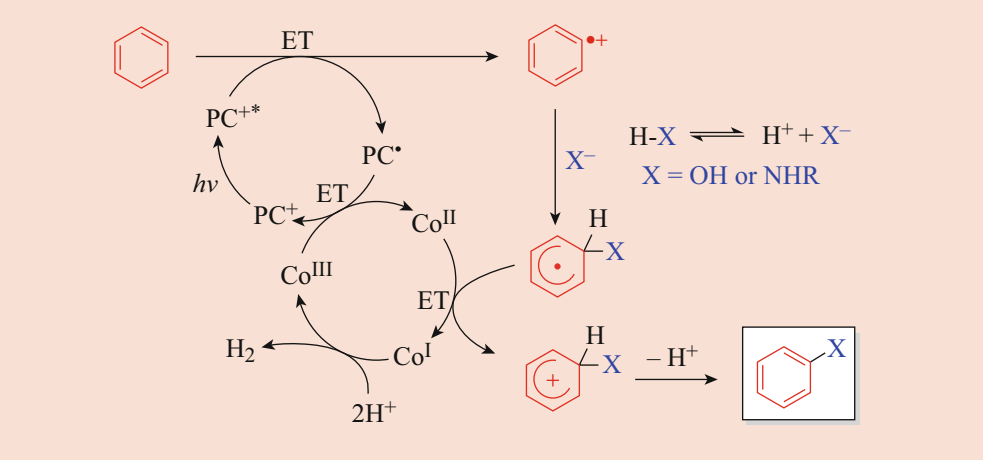

Fig. 46.13 The overall catalytic cycle for the photocatalytic hydrogen evolution with benzene, H-X ($X^- = OH^-$ and NHR^-), $QuCN^+$, and $Co^{II}(dmgBF_2)_2$. (Reprinted with permission from Ref. [98]. Copyright 2016, American Chemical Society)

(E_{ox} vs. SCE = 2.32 V) [100]. The occurrence of electron transfer from benzene to $^1QuCN^+$* was confirmed by laser-induced transient absorption spectra as shown in Fig. 46.14a, where the transient absorption bands due to quinolinyl radical ($QuCN^•$) and benzene dimer radical cation were observed at 520 nm and in the near-IR region, respectively. It is known that benzene radical cation is converted to benzene dimer radical cation by π-π association of benzene radical cation with large excess of benzene with the formation constant of 12 M^{-1} [101]. The rate constant of electron transfer from benzene to $^1QuCN^+$* to produce benzene dimer radical cation was determined from the linear plot in Fig. 46.14b to be $2.1 \times 10^{10}\ M^{-1}\ s^{-1}$, which is close to be the diffusion limited value in MeCN as expected from the exergonic electron transfer [102].

Acr^+-Mes in Fig. 46.5 can also be applied to photocatalytic generation of H_2, accompanied by dehydrogenative oxygenation of an alkene with $Co^{II}(dmgH)_2py$ [103]. The photocatalytic reaction is started by photoexcitation of Acr^+–Mes to produce the ET state, $Acr^•$–$Mes^{•+}$, followed by electron transfer from alkenes to the $Mes^{•+}$ moiety of $Acr^•$–$Mes^{•+}$ to produce the alkene radical cation and $Acr^•$–Mes. The alkene radical cation reacts with H_2O to produce the OH adduct radical after the deprotonation. The OH adduct radical is oxidized by $Co^{III}(dmgH)_2pyCl$ (or $Acr^•$–$Mes^{•+}$) to produce the carbonyl compound after the deprotonation. $Acr^•$–Mes can reduce $Co^{II}(dmgH)_2py$ to $[Co^{I}(dmgH)_2py]^-$ that reacts with H^+ to produce the Co (III)-hydride species, followed by the reaction with H^+ to produce H_2 and $Co^{III}(dmgH)_2pyCl$ [103]. Based on the catalytic cycle in Fig. 46.15, a number of alkenes are oxygenated by water (Eq. 46.4) in the presence of Acr^+–Mes and $Co^{II}(dmgH)_2py$ as a photocatalyst and a hydrogen evolution catalyst, respectively [103]. This dual catalytic system possesses the single anti-Markovnikov selectivity

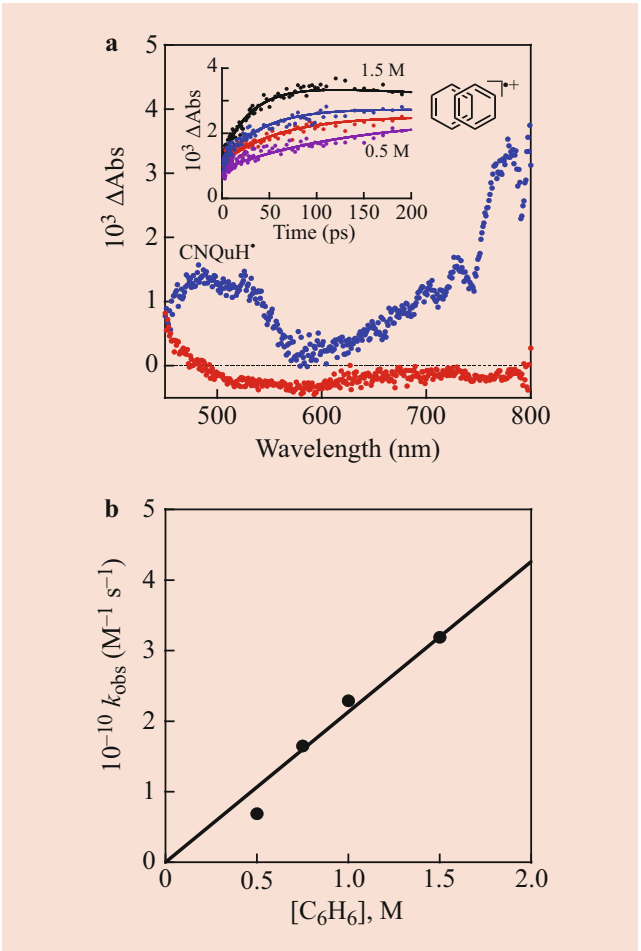

Fig. 46.14 (**a**) Transient absorption spectra of $QuCN^+$ in the absence (red dots) and presence (1.5 M, blue dots) of benzene in deaerated MeCN taken at 200 ps after femtosecond laser excitation (λ_{ex} = 355 nm). (**b**) Plot of the observed rate constant (k_{obs}) of formation of benzene dimer radical cation vs. [C_6H_6]. (Reprinted with permission from Ref. [102]. Copyright 2001, American Chemical Society)

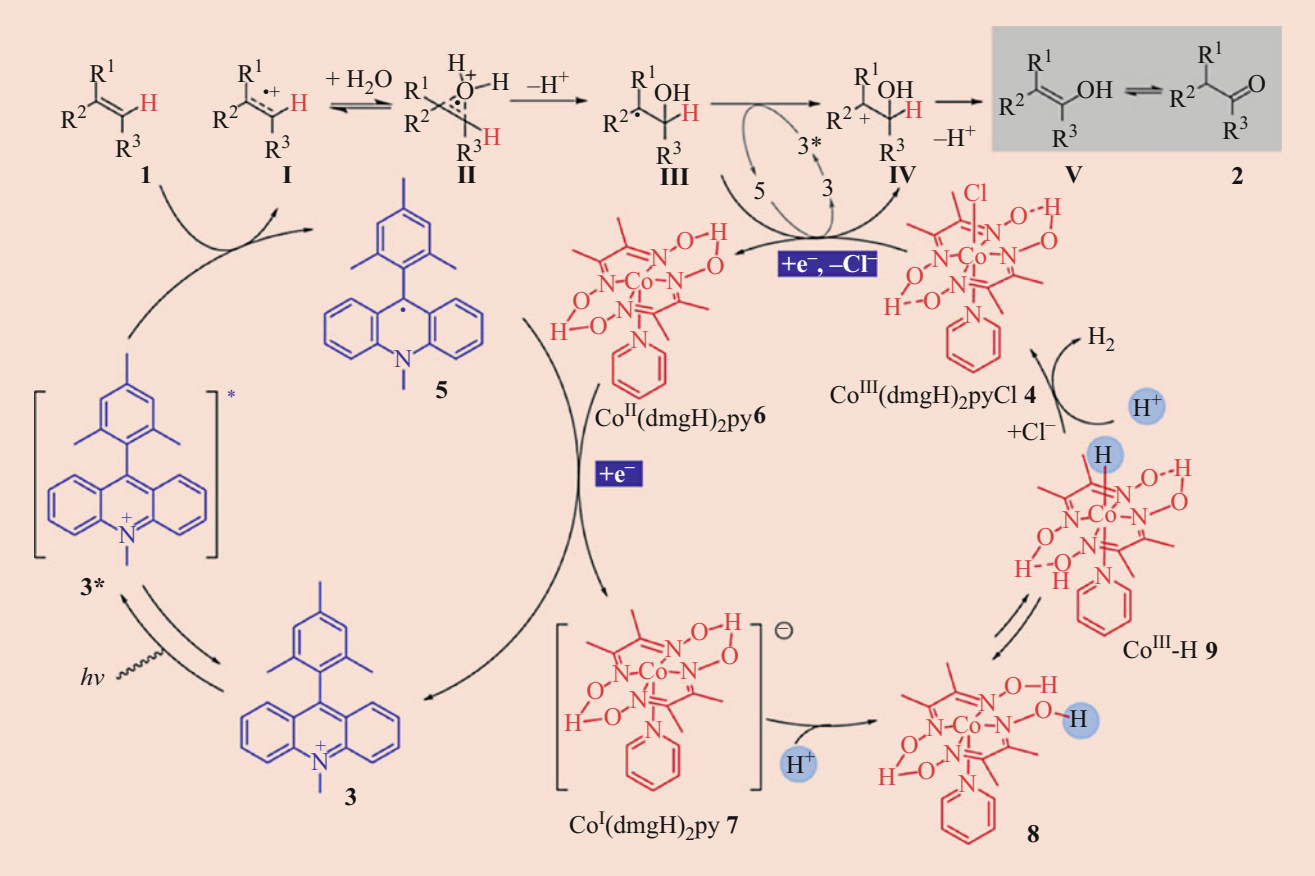

Fig. 46.15 The overall catalytic cycle for the photocatalytic hydrogen evolution coupled by oxygenation of alkenes with H_2O in the presence of Acr^+–Mes and $Co^{II}(dmgH)_2py$. (Reprinted with permission from Ref. [103]. Copyright 2016, American Chemical Society)

due to the property of the visible light-induced alkene radical cation intermediate [103].

$$R_1R_2C=C(H)R_3 + H_2O \xrightarrow[Acr^+-Mes,Co^{II}(dmgH)_2py]{h\nu} R_1R_2C(CO)R_3 + H_2 \quad (46.4)$$

In Fig. 46.15, the alkene radical cation reacts with a nucleophile (H_2O) to undergo C-O bond formation following photoinduced electron transfer from the alkene to $Acr^{\bullet}$–$Mes^{\bullet+}$. In the case of styrene, styrene radical cation undergoes the C-C bond formation by the dimerization with neutral syrene to produce the dimer radical cation following photoinduced electron transfer from the alkene to $Acr^{\bullet}$–$Mes^{\bullet+}$ as shown in Fig. 46.16 [104]. The syrene dimer radical cation undergoes deprotonation to produce the neutral radical that is oxidized by the Co(II) complex to yield the dimerized product after deprotonation [104]. The maximum yield of 1-phenyl-1,2-dihydronaphthalene was 72% in the presence of NaH_2PO_4 that acts as a good proton acceptor. Other photocatalysts such as rose bengal, rhodamine B, [Ir(dtbbpy)(ppy)$_2$][PF_6], eosin Y, and [Ru(bpy)$_3$]Cl_2 did not afford the desired product at all. In the control experiments, no desired product was observed without the organic redox catalyst, Acr^+–Mes, cobalt catalyst, or visible light, indicating that Acr^+–Mes and cobalt catalysts are essential for this transformation [104].

A selective C(sp^2)-H amination of arenes (alkyl-substituted benzenes, biphenyl, and anisole derivatives) accompanied by hydrogen evolution by using heterocyclic azoles as nitrogen sources has also been made possible by using Acr^+-Mes/cobalt catalyst as shown in Fig. 46.17 [105]. Methylarenes such as *p*-xylene can be oxidized by electron transfer to the $Mes^{\bullet+}$ moiety of $Acr^{\bullet}$–$Mes^{\bullet+}$ produced upon photoexcitation of Acr^+–Mes to produce *p*-xylene radical cation, which is attacked by nucleophile pyrazole (E_{ox} = 2.27 V vs. SCE), which is difficult to be oxidized by $Acr^{\bullet}$–$Mes^{\bullet+}$ (E_{red} = 2.06 V vs. SCE), to produce the radical adduct. Then, the radical adduct is oxidized by electron transfer to Co(II) catalyst, which quickly loses one proton and generates the amination product. At the same time,

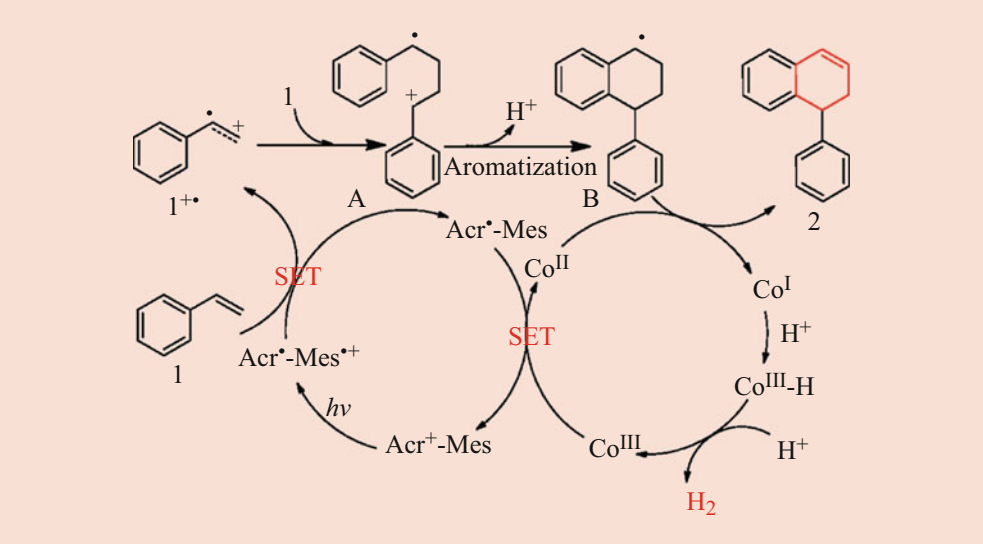

Fig. 46.16 The overall catalytic cycle for the photocatalytic hydrogen evolution with dimerization of styrenes in the presence of Acr^+–Mes and $Co^{II}(dmgH)_2py$. (Reprinted with permission from Ref. [104]. Copyright 2018, Elsevier)

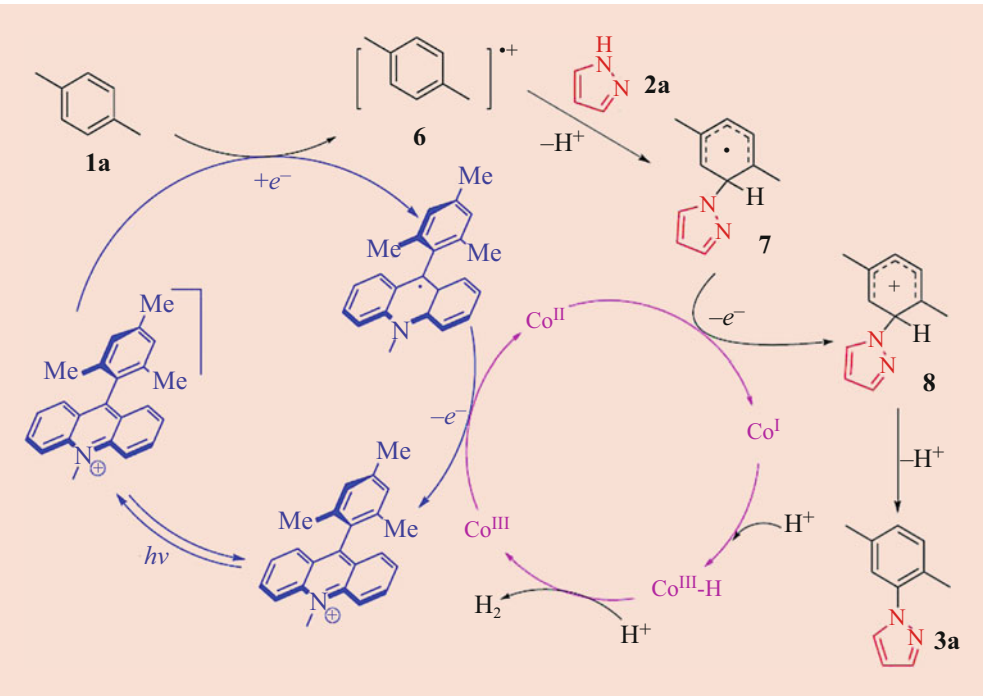

Fig. 46.17 The overall catalytic cycle for the photocatalytic hydrogen evolution with cross-coupling between simple arenes and heterocyclic amines in the presence of Acr^+–Mes and $Co^{II}(dmgH)_2py$. (Reprinted with permission from Ref. [105]. Copyright 2017, Springer Nature)

Co(I) could capture the present proton to produce Co(III)-H that reacts with H^+ to release H_2, accompanied by regeneration of the Co(III) complex.

46.7 One Photon-Two Electron Excitation

Photoexcitation of $[Cp^*Ir^{III}(bpy)H]^+$ results in a one photon-two electron process to produce $[Cp^*Ir^{I}(bpy)]$ and H^+ [106]. Before releasing H^+, the bimolecular reaction of the excited state of $[Cp^*Ir^{III}(bpy)H]^+$, which is equivalent to the $[Cp^*Ir^{I}(bpy)]/H^+$ pair, with $[Cp^*Ir^{III}(bpy)H]^+$ occurs to produce H_2, $[Cp^*Ir^{III}(bpy)(CH_3CN)]^{2+}$, and $[Cp^*Ir^{I}(bpy)]$ as shown in Fig. 46.18, where $[Cp^*Ir^{I}(bpy)]$ reacts with H^+ to regenerate $[Cp^*Ir^{III}(bpy)H]^+$ [107]. The quantum yield of photochemical H_2 production from $[Cp^*Ir^{III}(bpy)H]^+$ increased with an increase in concentration of $[Cp^*Ir^{III}(bpy)H]^+$ to reach 100% [100]. $[Cp^*Ir^{III}(bpy)H]^+$ may act as an efficient photoredox catalyst for H_2 generation via a one photon-two electron process.

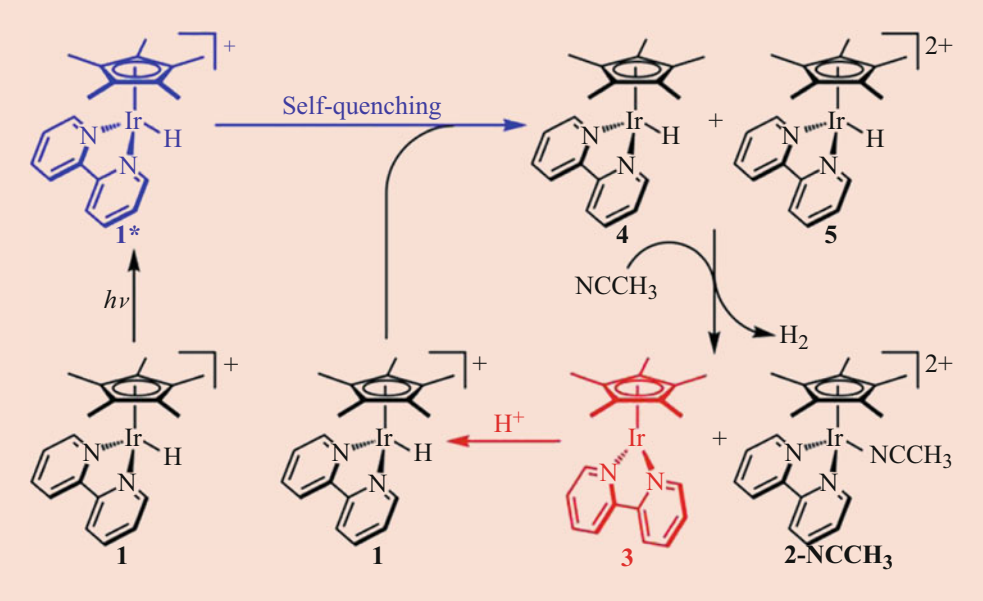

Fig. 46.18 Proposed mechanism of photochemical production of H_2 from $[Cp^*Ir^{III}(bpy)H]^+$. (Reprinted with permission from Ref. [107]. Copyright 2016, American Chemical Society)

46.8 Conclusion, Challenge, and Future Perspective

In order to produce hydrogen from two protons, two photons are generally required by conversion of two photons to two electrons. However, as shown in this chapter, only one photon is enough to produce hydrogen via photoinduced electron transfer followed by disproportionation of a redox catalyst to produce two-electron reduced species. Photoinduced electron transfer can be combined with thermal electron transfer to provide two electrons from one photon, leading to hydrogen production from protons. Depending on a type of electron donor substrate, the substrate radical cation produced by photoinduced electron transfer to a photoredox catalyst undergoes bond cleavage or bond formation to produce a much stronger electron donor to provide the second electron for hydrogen production from protons. Photoredox catalysts normally provide only one electron via photoinduced electron transfer of the photoexcited state. In the case of $[Cp^*Ir^{III}(bpy)H]^+$, however, the photoexcitation results in a one photon-two electron process to produce hydrogen via self-quenching with 100% quantum yield.

In the natural photosynthesis, $NADP^+$ is reduced by plastoquinol to produce NADPH in photosystem I [108, 109]. It is desired to develop efficient photocatalytic systems for hydrogen evolution from plastoquinol analogs to mimic the function of photosystem I by optimizing the conditions where photons are used to produce hydrogen as discussed in this chapter. On the other hand, water is oxidized by plastoquinone to produce O_2 and plastoquinol in photosystem II [110]. A molecular photocatalytic system to mimic the function of photosystem II has recently been reported to oxidize water by plastoquinone analogs to produce O_2 and plastoquinol analogs [111]. Thus, combination of such a molecular photocatalytic system to mimic photosystem II with a molecular photocatalytic system to mimic photosystem I may enable to produce hydrogen from water more efficiently than the natural system in future. The biggest challenge to use a molecular photocatalyst for H_2 evolution is the photostability because organic compounds are susceptible to the photoredox reactions, which cause degradation of the photocatalyst. Incorporation of a molecular photocatalyst into mesoporous silica alumina is reported to improve the photostability, because the immobilization of the catalyst prohibits the intermolecular reaction, which is the main reason of the photodegradation [112]. Construction of such immobilized molecular photocatalysts may provide more practical applications of molecular photocatalysts for hydrogen evolution.

Acknowledgments
The authors gratefully acknowledge the contributions of their collaborators and coworkers mentioned in the cited references, and financial supports from a SENTAN project from JST and JSPS KAKENHI (Grant Numbers 16H02268 to S.F.) from MEXT, Japan, and from the NRF of Korea through CRI (NRF-2021R1A3B1076539 to W.N), GRL (NRF-2010-00353 to W.N.), and Basic Science Research Program (2020R1I1A1A01074630 to Y.M.L. and 2017R1D1A1B03032615 to S.F.).

References

1. Yilmaz, F., Balta, M.T., Selbas, R.A.: A review of solar based hydrogen production methods. Renew. Sustain. Energy Rev. **56**, 171–178 (2016)
2. Bellani, S., Antognazza, M.R., Bonaccorso, F.: Carbon-based photocathode materials for solar hydrogen production. Adv. Mater. **31**, 1801446 (2019)
3. Nocera, D.G.: The artificial leaf. Acc. Chem. Res. **45**, 767–776 (2012)
4. Ashford, D.L., Gish, M.K., Vannucci, A.K., Brennaman, M.K., Templeton, J.L., Papanikolas, J.M., Meyer, T.J.: Molecular chromophore–catalyst assemblies for solar fuel applications. Chem. Rev. **115**, 13006–13049 (2015)
5. Yu, Z., Li, F., Sun, L.: Recent advances in dye-sensitized photoelectrochemical cells for solar hydrogen production based on molecular components. Energy Environ. Sci. **8**, 760–775 (2015)
6. Fukuzumi, S.: Artificial photosynthetic systems for production of hydrogen. Curr. Opin. Chem. Biol. **25**, 18–26 (2015)
7. Jacobsson, T.J., Fjällström, V., Edoff, M., Edvinsson, T.: Sustainable solar hydrogen production: from photoelectrochemical cells to PV-electrolyzers and back again. Energy Environ. Sci. **7**, 2056–2070 (2014)
8. Fukuzumi, S., Yamada, Y., Suenobu, T., Ohkubo, K., Kotani, H.: Catalytic mechanisms of hydrogen evolution with homogeneous and heterogeneous catalysts. Energy Environ. Sci. **4**, 2754–2766 (2011)
9. Cook, T.R., Dogutan, D.K., Reece, S.Y., Surendranath, Y., Teets, T.S., Nocera, D.G.: Solar energy supply and storage for the legacy and nonlegacy worlds. Chem. Rev. **110**, 6474–6502 (2010)
10. Walter, M.G., Warren, E.L., McKone, J.R., Boettcher, S.W., Mi, Q., Santori, E.A., Lewis, N.S.: Solar water splitting cells. Chem. Rev. **110**, 6446–6473 (2010)
11. Armaroli, N., Balzani, V.: The hydrogen issue. ChemSusChem. **4**, 21–36 (2011)
12. Ozawa, H., Sakai, K.: Photo-hydrogen-evolving molecular devices driving visible-light-induced water reduction into molecular hydrogen: structure–activity relationship and reaction mechanism. Chem. Commun. **47**, 2227–2242 (2011)
13. Eckenhoff, W.T., Eisenberg, R.: Molecular systems for light driven hydrogen production. Dalton Trans. **41**, 13004–13021 (2012)
14. Fukuzumi, S.: Bioinspired energy conversion systems for hydrogen production and storage. Eur. J. Inorg. Chem. (9), 1351–1362 (2008)
15. Turner, J.A.: Sustainable hydrogen production. Science. **305**, 972–974 (2004)
16. Yuan, Y.-J., Yu, Z.-T., Chen, D.-Q., Zou, Z.-G.: Metal-complex chromophores for solar hydrogen generation. Chem. Soc. Rev. **46**, 603–631 (2017)
17. Fukuzumi, S., Lee, Y.-M., Nam, W.: Thermal and photocatalytic production of hydrogen with earth-abundant metal complexes. Coord. Chem. Rev. **355**, 54–73 (2018)
18. Wang, Y., Suzuki, H., Xie, J., Tomita, O., Martin, D.J., Higashi, M., Kong, D., Abe, R., Tang, J.: Mimicking natural photosynthesis: solar to renewable H_2 fuel synthesis by Z-scheme water splitting systems. Chem. Rev. **118**, 5201–5241 (2018)
19. Eckenhoff, W.T.: Molecular catalysts of co, Ni, Fe, and Mo for hydrogen generation in artificial photosynthetic systems. Coord. Chem. Rev. **373**, 295–316 (2018)
20. Luo, G.-G., Pan, Z.-H., Lin, J.-Q., Sun, D.: Tethered sensitizer-catalyst Noble-metal-free molecular devices for solar-driven hydrogen generation. Dalton Trans. **47**, 15633–15645 (2018)
21. Pannwitz, A., Wenger, O.S.: Proton-coupled multi-Electron transfer and its relevance for artificial photosynthesis and photoredox catalysis. Chem. Commun. **55**, 4004–4014 (2019)
22. Nocera, D.G.: Solar fuels and solar chemicals industry. Acc. Chem. Res. **50**, 616–619 (2017)
23. Dalle, K.E., Warnan, J., Leung, J.J., Reuillard, B., Karmel, I.S., Reisner, E.: Electro- and solar-driven fuel synthesis with first row transition metal complexes. Chem. Rev. **119**, 2752–2875 (2019)
24. Zhang, B., Sun, L.: Artificial photosynthesis: opportunities and challenges of molecular catalysts. Chem. Soc. Rev. **48**, 2216–2264 (2019)
25. Fukuzumi, S.: Production of liquid solar fuels and their use in fuel cells. Joule. **1**, 689–738 (2017)
26. Jia, J., Seitz, L.C., Benck, J.D., Huo, Y., Chen, Y., Ng, J.W.D., Bilir, T., Harris, J.S., Jaramillo, T.F.: Solar water splitting by photovoltaic-electrolysis with a solar-to-hydrogen efficiency over 30%. Nat. Commun. **7**, 13237 (2016)
27. Prier, C.K., Rankic, D.A., MacMillan, D.W.C.: Visible light photoredox catalysis with transition metal complexes: applications in organic synthesis. Chem. Rev. **113**, 5322–5363 (2013)
28. Fukuzumi, S., Ohkubo, K.: Selective photocatalytic reactions with organic photocatalysts. Chem. Sci. **4**, 561–574 (2013)
29. Fukuzumi, S., Ohkubo, K.: Organic synthetic transformations using organic dyes as photoredox catalysts. Org. Biomol. Chem. **12**, 6059–6071 (2014)
30. Romero, N.A., Nicewicz, D.A.: Organic photoredox catalysis. Chem. Rev. **116**, 10075–10166 (2016)
31. Wang, C.-S., Dixneuf, P.H., Soulé, J.-F.: Photoredox catalysis for building C−C bonds from $C(sp^2)$–H bonds. Chem. Rev. **118**, 7532–7585 (2018)
32. Marzo, L., Pagire, S.K., Reiser, O., König, B.: Visible-light photocatalysis: does it make a difference in organic synthesis? Angew. Chem. Int. Ed. **57**, 10034–10072 (2018)
33. Wang, H., Gao, X., Lv, Z., Abdelilah, T., Lei, A.: Recent advances in oxidative R_1-H/R_2-H cross-coupling with hydrogen evolution via photo-/electrochemistry. Chem. Rev. **119**(12), 6769–6787 (2019). https://doi.org/10.1021/acs.chemrev.9b00045
34. Juris, A., Balzani, V., Barigelletti, F., Campagna, S., Belser, P., von Zelewsky, A.: Ru(II) polypyridine complexes: photophysics, photochemistry, electrochemistry, and chemiluminescence. Coord. Chem. Rev. **84**, 85–277 (1988)
35. Grätzel, M.: Artificial photosynthesis: water cleavage into hydrogen and oxygen by visible light. Acc. Chem. Res. **14**, 376–384 (1981)
36. Kiwi, J., Grätzel, M.: Hydrogen evolution from water induced by visible light mediated by redox catalysis. Nature. **281**, 657–658 (1979)
37. Okura, I.: Hydrogenase and its application for photoinduced hydrogen evolution. Coord. Chem. Rev. **68**, 53–99 (1985)
38. Ladomenou, K., Natali, M., Iengo, E., Charalampidis, G., Scandola, F., Coutsolelos, A.G.: Photochemical hydrogen generation with porphyrin-based systems. Coord. Chem. Rev. **304-305**, 38–54 (2015)
39. Nurttila, S.S., Becker, R., Hessels, J., Woutersen, S., Reek, J.N.H.: Photocatalytic hydrogen evolution by a synthetic [FeFe] hydrogenase mimic encapsulated in a porphyrin cage. Chem. Eur. J. **24**, 16395–16406 (2018)
40. Mills, I.N., Porras, J.A., Bernhard, S.: Judicious design of cationic, cyclometalated Ir(III) complexes for photochemical energy conversion and optoelectronics. Acc. Chem. Res. **51**, 352–364 (2018)
41. Porras, J.A., Mills, I.N., Transue, W.J., Bernhard, S.: Highly fluorinated Ir(III)−2,2′:6′,2″-terpyridine-phenylpyridine-X complexes via selective C–F activation: robust photocatalysts for solar fuel generation and photoredox catalysis. J. Am. Chem. Soc. **138**, 9460–9472 (2016)

42. Torres, J., Carrión, M.C., Leal, J., Jalón, F.A., Cuevas, J.V., Rodríguez, A.M., Castañeda, G., Manzano, B.R.: Cationic bis (cyclometalated) Ir(III) complexes with pyridine–carbene ligands. Photophysical properties and photocatalytic hydrogen production from water. Inorg. Chem. **57**, 970–984 (2018)
43. Han, Z., Eisenberg, R.: Fuel from water: the photochemical generation of hydrogen from water. Acc. Chem. Res. **2014**(47), 2537–2544 (2014)
44. Dong, R., Chen, K.-K., Wang, P., Zhang, N., Guo, S., Zhang, Z.-M., Lu, T.-B.: Heavy atom-free keto-di-coumarin as earth-abundant strong visible light-harvesting photosensitizer for efficient photocatalytic hydrogen evolution. Dyes Pigments. **166**, 84–91 (2019)
45. Archer, S., Weinstein, J.A.: Charge-separated excited states in platinum(II) chromophores: photophysics, formation, stabilization and utilization in solar energy conversion. Coord. Chem. Rev. **256**, 2530–2561 (2012)
46. Du, P., Knowles, K., Eisenberg, R.: A homogeneous system for the photogeneration of hydrogen from water based on a platinum (II) terpyridyl acetylide chromophore and a molecular cobalt catalyst. J. Am. Chem. Soc. **130**, 12576–12577 (2008)
47. Zarkadoulas, A., Koutsouri, E., Kefalidi, C., Mitsopoulou, C.A.: Rhenium complexes in homogeneous hydrogen evolution. Coord. Chem. Rev. **304–305**, 55–72 (2015)
48. Mara, M.W., Fransted, K.A., Chen, L.X.: Interplays of excited state structures and dynamics in copper(I) diimine complexes: implications and perspectives. Coord. Chem. Rev. **282–283**, 2–18 (2015)
49. Windisch, J., Orazietti, M., Hamm, P., Alberto, R., Probst, B.: General scheme for oxidative quenching of a copper bis-phenanthroline photosensitizer for light-driven hydrogen production. ChemSusChem. **9**, 1719–1726 (2016)
50. Zhang, Y., Schulz, M., Wächtler, M., Karnahl, M., Dietzek, B.: Heteroleptic diimine–diphosphine Cu(I) complexes as an alternative towards noble-metal based photosensitizers: design strategies, photophysical properties and perspective applications. Coord. Chem. Rev. **356**, 127–146 (2018)
51. Saeedi, S., Xue, C., McCullough, B.J., Roe, S.E., Neyhouse, B.J., White, T.A.: Probing the diphosphine ligand's impact within heteroleptic, visible-light-absorbing cu(I) photosensitizers for solar fuels production. ACS Appl. Energy Mater. **2**, 131–143 (2019)
52. Fukuzumi, S., Yamada, Y.: Catalytic activity of metal-based nanoparticles for photocatalytic water oxidation and reduction. J. Mater. Chem. **22**, 24284–24296 (2012)
53. Pellegrin, Y., Odobel, F.: Sacrificial electron donor reagents for solar fuel production. C. R. Chimie. **20**, 283–295 (2017)
54. Harriman, H.: Metalloporphyrin-photosensitized formation of hydrogen from organic and inorganic substrates. J. Photochem. **29**, 139–150 (1985)
55. Okura, I.: Application of hydrogenase for photoinduced hydrogen evolution. Biochimie. **68**, 189–199 (1986)
56. Wombwell, C., Caputo, C.A., Reisner, E.: [NiFeSe]-hydrogenase chemistry. Acc. Chem. Res. **48**, 2858–2865 (2015)
57. Lee, S.H., Choi, D.S., Kuk, S.K., Park, C.B.: Photobiocatalysis: activating redox enzymes by direct or indirect transfer of photoinduced electrons. Angew. Chem. Int. Ed. **57**, 7958–7985 (2018)
58. Gartner, F., Sundararaju, B., Surkus, A.E., Boddien, A., Loges, B., Junge, H., Dixneuf, P.H., Beller, M.: Light-driven hydrogen generation: efficient Iron-based water reduction catalysts. Angew. Chem. Int. Ed. **48**, 9962–9965 (2009)
59. Junge, H., Rockstroh, N., Fischer, S., Brückner, A., Ludwig, R., Lochbrunner, S., Kühn, O., Beller, M.: Light to hydrogen: photocatalytic hydrogen generation from water with molecularly-defined Iron complexes. Inorganics. **5**, 14 (2017). https://doi.org/10.3390/inorganics5010014
60. Ho, X.L., Shao, H., Ng, Y.Y., Ganguly, R., Lu, Y., Soo, H.S.: Visible light driven hydrogen evolution by molecular nickel catalysts with time-resolved spectroscopic and DFT insights. Inorg. Chem. **58**, 1469–1480 (2019)
61. Koshiba, K., Yamauchi, K., Sakai, K.: A nickel dithiolate water reduction catalyst providing ligand-based proton-coupled electron-transfer pathways. Angew. Chem. Int. Ed. **56**, 4247–4251 (2017)
62. Gross, M.A., Reynal, A., Durrant, J.R., Reisner, E.: Versatile photocatalytic systems for H_2 generation in water based on an efficient DuBois-type nickel catalyst. J. Am. Chem. Soc. **136**, 356–366 (2014)
63. Han, Z., Shen, L., Brennessel, W.W., Holland, P.L., Eisenberg, R.: Nickel pyridinethiolate complexes as catalysts for the light-driven production of hydrogen from aqueous solutions in noble-metal-free systems. J. Am. Chem. Soc. **135**, 14659–14669 (2013)
64. Hong, D., Tsukakoshi, Y., Kotani, H., Ishizuka, T., Ohkubo, K., Shiota, Y., Yoshizawa, K., Fukuzumi, S., Kojima, T.: Mechanistic insights into homogeneous electrocatalytic and photocatalytic hydrogen evolution catalyzed by high-spin Ni(II) complexes with S_2N_2-type tetradentate ligands. Inorg. Chem. **57**, 7180–7190 (2018)
65. Sakai, K., Ozawa, H.: Homogeneous catalysis of platinum (II) complexes in photochemical hydrogen production from water. Coord. Chem. Rev. **251**, 2753–2766 (2007)
66. Lang, P., Habermehl, J., Troyanov, S.I., Rau, S., Schwalbe, M.: Photocatalytic generation of hydrogen using dinuclear π-extended porphyrin–platinum compounds. Chem. Eur. J. **24**, 3225–3233 (2018)
67. Kaeffer, N., Chavarot-Kerlidou, M., Artero, V.: Hydrogen evolution catalyzed by cobalt diimine–dioxime complexes. Acc. Chem. Res. **48**, 1286–1295 (2015)
68. Mulfort, K.L.: Interrogation of cobaloxime-based supramolecular photocatalyst architectures. C. R. Chimie. **20**, 221–229 (2017)
69. Queyriaux, N., Jane, R.T., Massin, J., Artero, V., Chavarot-Kerlidou, M.: Recent developments in hydrogen evolving molecular cobalt(II)–polypyridyl catalysts. Coord. Chem. Rev. **304-305**, 3–19 (2015)
70. Losse, S., Vos, J.G., Rau, S.: Catalytic hydrogen production at cobalt centres. Coord. Chem. Rev. **254**, 2492–2504 (2010)
71. Stoll, T., Castillo, C.E., Kayanuma, M., Sandroni, M., Daniel, C., Odobel, F., Fortage, J., Collomb, M.-N.: Photo-induced redox catalysis for proton reduction to hydrogen with homogeneous molecular systems using rhodium-based catalysts. Coord. Chem. Rev. **304-305**, 20–37 (2015)
72. Manbeck, G.F., Fujita, E., Brewer, K.J.: Tetra- and heptametallic Ru(II), Rh(III) supramolecular hydrogen production photocatalysts. J. Am. Chem. Soc. **139**, 7843–7854 (2017)
73. McCullough, B.J., Neyhouse, B.J., Schrage, B.R., Reed, D.T., Osinski, A.J., Ziegler, C.J., White, T.A.: Visible-light-driven photosystems using heteroleptic cu(I) photosensitizers and Rh(III) catalysts to produce H_2. Inorg. Chem. **57**, 2865–2875 (2018)
74. Kataoka, Y., Yano, N., Handa, M., Kawamoto, T.: Intrinsic hydrogen evolution capability and a theoretically supported reaction mechanism of a paddlewheel-type dirhodium complex. Dalton Trans. **48**, 7302–7312 (2019)
75. Fukuzumi, S., Kobayashi, T., Suenobu, T.: Efficient catalytic decomposition of formic acid for the selective generation of H_2 and H/D exchange with a water-soluble rhodium complex in aqueous solution. ChemSusChem. **1**, 827–834 (2008)
76. Fukuzumi, S., Kobayashi, T., Suenobu, T.: Unusually large tunneling effect on highly efficient generation of hydrogen and hydrogen isotopes in pH-selective decomposition of formic acid catalyzed by a heterodinuclear iridium-ruthenium complex in water. J. Am. Chem. Soc. **132**, 1496–1497 (2010)
77. Fukuzumi, S., Kobayashi, T., Suenobu, T.: Photocatalytic production of hydrogen by disproportionation of one-electron-reduced

rhodium and iridium–ruthenium complexes in water. Angew. Chem. Int. Ed. **50**, 728–731 (2011)
78. Grass, V., Lexa, D., Momenteau, M., Savéant, J.-M.: Reductive electrochemistry of rhodium porphyrins. Disproportionation of intermediary oxidation states. J. Am. Chem. Soc. **119**, 3536–3542 (1997)
79. Castillo, C.E., Stoll, T., Sandroni, M., Gueret, R., Fortage, J., Kayanuma, M., Daniel, C., Odobel, F., Deronzier, A., Collomb, M.-N.: Electrochemical generation and spectroscopic characterization of the key rhodium(III) hydride intermediates of rhodium poly (bipyridyl) H_2-evolving catalysts. Inorg. Chem. **57**, 11225–11239 (2018)
80. Kayanuma, M., Stoll, T., Daniel, C., Odobel, F., Fortage, J., Deronzier, A., Collom, M.-N.: A computational mechanistic investigation of hydrogen production in water using the $[Rh^{III}(dmbpy)_2Cl_2]^+$/$[Ru^{II}(bpy)_3]^{2+}$/ascorbic acid photocatalytic system. Phys. Chem. Chem. Phys. **17**, 10497–10509 (2015)
81. Aoi, S., Mase, K., Ohkubo, K., Fukuzumi, S.: Mechanism of a one-photon two-electron process in photocatalytic hydrogen evolution from ascorbic acid with a cobalt chlorin complex. Chem. Commun. **51**, 15145–15148 (2015)
82. Mandal, S., Shikano, S., Yamada, Y., Lee, Y.-M., Nam, W., Llobet, A., Fukuzumi, S.: Protonation equilibrium and hydrogen production by a dinuclear co-Hbpp complex reduced by cobaltocene with trifluoroacetic acid. J. Am. Chem. Soc. **135**, 15294–15297 (2013)
83. Beyene, B.B., Hung, C.-H.: Photocatalytic hydrogen evolution from neutral aqueous solution by a water-soluble cobalt (II) porphyrin. Sustain. Energy Fuels. **2**, 2036–2043 (2018)
84. Leung, C.-F., Cheng, S.-C., Yang, Y., Xiang, J., Yiu, S.-M., Ko, C.-C., Lau, T.-C.: Efficient photocatalytic water reduction by a cobalt (III) tripodal iminopyridine complex. Cat. Sci. Technol. **8**, 307–313 (2018)
85. Fukuzumi, S., Kotani, H., Ohkubo, K., Ogo, S., Tkachenko, N.V., Lemmetyinen, H.: Electron-transfer state of 9-mesityl-10-methylacridinium ion with a much longer lifetime and higher energy than that of natural photosynthetic reaction center. J. Am. Chem. Soc. **126**, 1600–1601 (2004)
86. Kotani, H., Ono, T., Ohkubo, K., Fukuzumi, S.: Efficient photocatalytic hydrogen evolution without an electron mediator using a simple electron donor–acceptor dyad. Phys. Chem. Chem. Phys. **9**, 1487–1492 (2007)
87. Fukuzumi, S., Ohkubo, K., Suenobu, T.: Long-lived charge separation and applications in artificial photosynthesis. Acc. Chem. Res. **47**, 1455–1464 (2014)
88. Tsudaka, T., Kotani, H., Ohkubo, K., Nakagawa, T., Tkachenko, N. V., Lemmetyinen, H., Fukuzumi, S.: Photoinduced electron transfer in 9-substituted 10-methylacridinium ions. Chem. Eur. J. **23**, 1306–1317 (2017)
89. Ohkubo, K., Mizushima, K., Iwata, R., Souma, K., Suzuki, N., Fukuzumi, S.: Simultaneous production of *p*-tolualdehyde and hydrogen peroxide in photocatalytic oxygenation of *p*-xylene and reduction of oxygen with 9-mesityl-10-methylacridinium ion derivatives. Chem. Commun. **46**, 601–603 (2010)
90. Fukuzumi, S., Tanaka, T.: in Photoinduced Electron Transfer, Part C, ed. M.A. Fox, M. Chanon, Elsevier, Amsterdam, 1988, ch. 10
91. Kotani, H., Hanazaki, R., Ohkubo, K., Yamada, Y., Fukuzumi, S.: Size- and shape-dependent activity of metal nanoparticles as hydrogen-evolution catalysts: mechanistic insights into photocatalytic hydrogen evolution. Chem. Eur. J. **17**, 2777–2785 (2010)
92. Kotani, H., Ohkubo, K., Fukuzumi, S.: Formation of a long-lived electron-transfer state of a naphthalene-quinolinium ion dyad and the π-dimer radical cation. Faraday Discuss. **155**, 89–102 (2012)
93. Yamada, Y., Miyahigashi, T., Kotani, H., Ohkubo, K., Fukuzumi, S.: Photocatalytic hydrogen evolution under highly basic conditions by using Ru nanoparticles and 2-phenyl-4-(1-naphthyl)quinolinium ion. J. Am. Chem. Soc. **133**, 16136–16145 (2011)
94. Yamada, Y., Miyahigashi, T., Kotani, H., Ohkubo, K., Fukuzumi, S.: Photocatalytic hydrogen evolution with Ni nanoparticles by using 2-Phenyl-4-(1-naphthyl)quinolinium ion as a photocatalyst. Energy Environ. Sci. **5**, 6111–6118 (2012)
95. Yamada, Y., Miyahigashi, T., Ohkubo, K., Fukuzumi, S.: Photocatalytic hydrogen evolution from carbon-neutral oxalate with 2-phenyl-4-(1-naphthyl)quinolinium ion and metal nanoparticles. Phys. Chem. Chem. Phys. **14**, 10564–10571 (2012)
96. Fukuzumi, S., Jung, J., Yamada, Y., Kojima, T., Nam, W.: Homogeneous and heterogeneous photocatalytic water oxidation by persulfate. Chem. Asian J. **11**, 1138–1150 (2016)
97. Yamada, Y., Oyama, K., Suenobu, T., Fukuzumi, S.: Photocatalytic water oxidation by persulphate with a Ca^{2+} ion-incorporated polymeric cobalt cyanide complex affording O_2 with 200% quantum efficiency. Chem. Commun. **53**, 3418–3421 (2017)
98. Zheng, Y.-W., Chen, B., Ye, P., Feng, K., Wang, W., Meng, Q.-Y., Wu, L.-Z., Tung, C.-H.: Photocatalytic hydrogen-evolution cross-couplings: benzene C–H amination and hydroxylation. J. Am. Chem. Soc. **138**, 10080–10083 (2016)
99. Ohkubo, K., Suga, K., Morikawa, K., Fukuzumi, S.: Selective oxygenation of ring-substituted toluenes with electron-donating and -withdrawing substituents by molecular oxygen via photoinduced electron transfer. J. Am. Chem. Soc. **125**, 12850–12859 (2003)
100. Ohkubo, K., Kobayashi, T., Fukuzumi, S.: Direct oxygenation of benzene to phenol using quinolinium ions as homogeneous photocatalysts. Angew. Chem. Int. Ed. **50**, 8652–8655 (2011)
101. Merkel, P.B., Luo, P., Dinnocenzo, J.P., Farid, S.: Accurate oxidation potentials of benzene and biphenyl derivatives via electron-transfer equilibria and transient kinetics. J. Org. Chem. **74**, 5163–5173 (2009)
102. Fukuzumi, S., Ohkubo, K., Suenobu, T., Kato, K., Fujitsuka, M., Ito, O.: Photoalkylation of 10-alkylacridinium ion via a charge-shift type of photoinduced electron transfer controlled by solvent polarity. J. Am. Chem. Soc. **123**, 8459–8467 (2001)
103. Zhang, G., Hu, X., Chiang, C.-W., Yi, H., Pei, P., Singh, A.K., Lei, A.: Anti-Markovnikov oxidation of β-alkyl styrenes with H_2O as the terminal oxidant. J. Am. Chem. Soc. **138**, 12037–12040 (2016)
104. Cao, W., Wu, C., Lei, T., Yang, X., Chen, B., Tung, C., Wu, L.: Photocatalytic hydrogen-evolution dimerization of styrenes to synthesize 1,2-Dihydro-1-arylnaphthalene derivatives using Acr^+-Mes and cobaloxime catalysts. Chin. J. Catal. **39**, 1194–1201 (2018)
105. Niu, L., Yi, H., Wang, S., Liu, T., Liu, J., Lei, A.: Photo-induced oxidant-free oxidative C–H/N–H cross-coupling between arenes and azoles. Nat. Commun. **8**, 14226 (2017)
106. Suenobu, T., Ogo, S., Fukuzumi, S.: Exited-state deprotonation and H/D exchange of an iridium hydride complex. Angew. Chem. Int. Ed. **42**, 5492–5495 (2003)
107. Chambers, M.B., Kurtz, D.A., Pitman, C.L., Brennaman, M.K., Miller, A.J.M.: Efficient photochemical dihydrogen generation initiated by a bimetallic self-quenching mechanism. J. Am. Chem. Soc. **138**, 13509–13512 (2016)
108. Najafpour, M.M., Renger, G., Hołyńska, M., Moghaddam, A.N., Aro, E.-M., Carpentier, R., Nishihara, N., Eaton-Rye, J.J., Shen, J.-R., Al-lakhverdiev, S.I.: Manganese compounds as water-oxidizing catalysts: from the natural water-oxidizing complex to nanosized manganese oxide structures. Chem. Rev. **116**, 2886–2936 (2016)
109. Caspy, I., Nelson, N.: Structure of the plant photosystem I. Biochem. Soc. Trans. **46**, 285–294 (2018)
110. Fukuzumi, S., Lee, Y.-M., Nam, W.: Mimicry and functions of photosynthetic reaction centers. Biochem. Soc. Trans. **46**, 1279–1288 (2018)

111. Hong, Y.H., Jung, J., Nakagawa, T., Sharma, N., Lee, Y.-M., Nam, W., Fukuzumi, S.: Photodriven oxidation of water by plastoquinone analogs with a nonheme iron catalyst. J. Am. Chem. Soc. **141**, 6748–6754 (2019)
112. Fukuzumi, S., Doi, K., Itoh, A., Suenobu, T., Ohkubo, K., Yamada, Y., Karlin, K.D.: Formation of a long-lived electron-transfer state in mesoporous silica-alumina composites enhances photocatalytic oxygenation reactivity. Proc. Natl. Acad. Sci. U. S. A. **109**, 15572–15577 (2012)

Shunichi Fukuzumi earned a bachelor's degree and Ph.D. degree in applied chemistry at Tokyo Institute of Technology in 1973 and 1978, respectively. After working as a postdoctoral fellow from 1978 to 1981 at Indiana University in the USA, he became an Assistant Professor in 1981 at Osaka University where he was promoted to a Full Professor in 1994. His research has focused on electron transfer chemistry, in particular artificial photosynthesis. He is currently a Distinguished Professor of Ewha Womans University, Korea, a Designated Professor of Meijo University, and a Professor Emeritus of Osaka University, Japan.

Yong-Min Lee received B.S., Master, and Ph.D. degrees in Chemistry under the supervision of Professor Sung-Nak Choi at Pusan National University, Republic of Korea in 1990, 1995, and 1999, respectively. After he worked in the Centro di Ricerca di Risonanze Magnetiche (CERM) at Università degli Studi di Firenze, Italia, as a Postdoctoral fellow and Researcher under the direction of Professors Ivano Bertini and Claudio Luchinat from 1999 to 2005, he joined the Centre for Biomimetic Systems at Ewha Womans University, as a Research Professor in 2006. He is currently a Special Appointment Professor at Ewha Womans University since 2009.

Wonwoo Nam earned his B.S. (Honors) degree in Chemistry from California State University, Los Angeles, and his Ph.D. degree in Inorganic Chemistry from University of California, Los Angeles (UCLA), under the supervision of Professor Joan S. Valentine in 1990. After working as a postdoctoral fellow at UCLA for 1 year, he became an Assistant Professor at Hong Ik University in 1991. In 1994, he moved to Ewha Womans University, where he is currently a Distinguished Professor. His current research has been focusing on the dioxygen activation, water oxidation, and important roles of metal ions in bioinorganic chemistry.